

Review

Overview of Low-Temperature Heat Capacity Data for $\text{Zn}_2(\text{C}_8\text{H}_4\text{O}_4)_2 \cdot \text{C}_6\text{H}_{12}\text{N}_2$ and the Salam Hypothesis

Svetlana Kozlova ^{1,2,*} , Maxim Ryzhikov ^{1,2} , Denis Pishchur ¹  and Irina Mirzaeva ^{1,2}

¹ Nikolaev Institute of Inorganic Chemistry, Siberian Branch, Russian Academy of Sciences, Lavrentyev Av., 3, RU-630090 Novosibirsk, Russia; maxim.ryzhikov@gmail.com (M.R.); denispishchur@ngs.ru (D.P.); dairdre@gmail.com (I.M.)

² Novosibirsk State University, Pirogova Street, 2, RU-630090 Novosibirsk, Russia

* Correspondence: sgk@niic.nsc.ru

Received: 29 March 2019; Accepted: 9 May 2019; Published: 11 May 2019



Abstract: The review presents the progress in the analysis of low-temperature heat capacity of the metal-organic framework $\text{Zn}_2(\text{C}_8\text{H}_4\text{O}_4)_2 \cdot \text{C}_6\text{H}_{12}\text{N}_2$ (Zn-DMOF). In Zn-DMOF, left-twisted $D_3(S)$ and right-twisted $D_3(R)$ DABCO molecules ($\text{C}_6\text{H}_{12}\text{N}_2$) can transform into each other by tunneling to form a racemate. Termination of tunneling leads to a phase transition in the subsystem of twisted molecules. It is suggested that Zn-DMOF may be considered a model system to study the mechanisms of phase transitions belonging to the same type as hypothetical Salam phase transitions.

Keywords: heat capacity; metal-organic framework; triethylenediamine (DABCO) molecules; racemate; Salam hypothesis

1. Introduction

According to the Salam hypothesis, a small parity-violating energy difference (PVED) between amino acid molecules along with the Bose-Einstein (BE) condensation, makes the less stable right enantiomers tunnel into the more stable left enantiomers, by changing their structural forms. This process was described as a second-order phase transition, which is an analog of the Bardeen-Cooper-Schrieffer (BCS) phase transition; therefore, physical properties such as heat capacity and magnetic susceptibility should change during this phase transition according to the BCS laws [1,2]. Even though no such phase transitions have been found in the crystals of known amino acids, the building material of living organisms, the systems demonstrating the BE condensation of chiral molecules are still of interest. A model of BE condensation was developed for a gas of non-interacting chiral molecules to determine the PVED contribution from low-temperature heat capacity data [3]. The present review summarizes low-temperature heat capacity data, which indicate that the BE condensation may work in a subsystem of triethylenediamine (DABCO) molecules ($\text{C}_6\text{H}_{12}\text{N}_2$) in the metal-organic framework $\text{Zn}_2(\text{C}_8\text{H}_4\text{O}_4)_2 \cdot \text{C}_6\text{H}_{12}\text{N}_2$ (Zn-DMOF) and that the mechanism of Salam phase transitions remains possible. In Zn-DMOF, the enantiomers are represented by left- and right-twisted DABCO molecules, which transform into each other as a result of tunneling.

2. Structure of DABCO Molecule in $\text{Zn}_2(\text{C}_8\text{H}_4\text{O}_4)_2 \cdot \text{C}_6\text{H}_{12}\text{N}_2$

Triethylenediamine (DABCO) appears in the form of two conformational isomers with D_{3h} and D_3 point group symmetries, depending on intermolecular interactions. Also, a quasi- D_{3h} form of DABCO is possible due to strong vibrations of the molecule around the C_3 axis. The molecules with the D_3 symmetry, which can be left-twisted $D_3(S)$ or right-twisted $D_3(R)$, are considered to be chiral isomers (enantiomers) [4].

Above 223 K, the crystal structure of the metal-organic framework Zn-DMOF is tetragonal, with space group $P4/mmm$ [5]. The horizontal planes are formed by terephthalate anions $[C_8H_4O_4]^{2-}$ (BDC^{2-}) which are linked to $\{Zn_2\}$ pairs by carboxylate anions. The vertical edges are formed by DABCO molecules (linkers), the point symmetry of which does not contain a 4-fold rotational symmetry axis (Figure 1). This is the reason why DABCO molecules are orientationally disordered; moreover, $D_3(S)$ and $D_3(R)$ forms can transform into each other (by activation or tunneling) [4,6]. Calorimetry, nuclear magnetic resonance, and X-ray structural analysis data provide evidence of the presence of phase transitions in Zn-DMOF at ~ 14 , ~ 60 , and ~ 130 K [7–12].

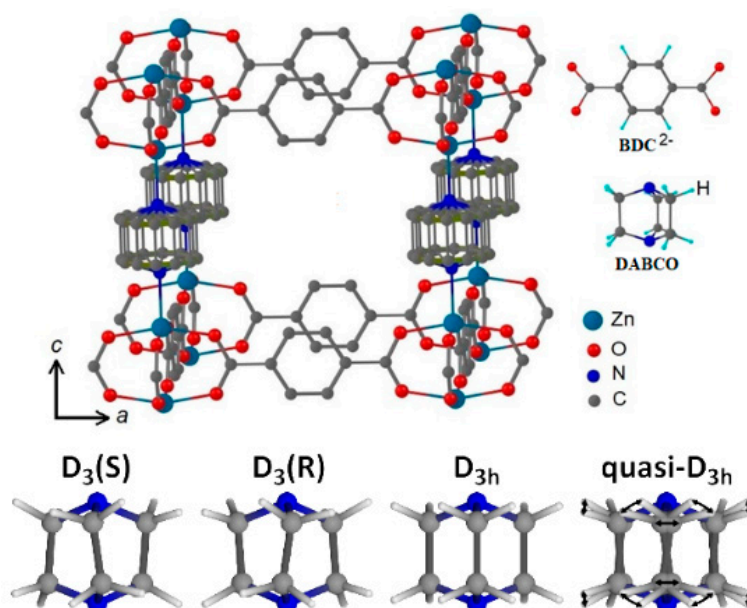


Figure 1. The structure of $Zn_2(C_8H_4O_4)_2 \cdot C_6H_{12}N_2$ (Zn-DMOF), space group $P4/mmm$. Positions of carbon atoms in triethylenediamine (DABCO) molecules are disordered [5]. Hydrogen atoms are omitted for clarity. DABCO and BDC^{2-} structures are shown in the insets. (Compiled from Figure 1 in [10] and Figure 1 in [1]).

3. Mobility of DABCO Molecules in $Zn_2(C_8H_4O_4)_2 \cdot C_6H_{12}N_2$

In Zn-DMOF, BDC^{2-} anions and DABCO molecules are involved in activation mobility. According to the nuclear magnetic resonance (NMR) studies of the activation mobility of BDC^{2-} anions, the $[C_6H_4]$ groups of BDC^{2-} anions rotate about the C_2 axis through an angle of 180° (flipping) [13–15]. No effect of BDC^{2-} flipping on the mobility of DABCO in Zn-DMOF was discovered [13,16,17].

According to the detailed analysis of the temperature behavior of the spin-lattice relaxation times of hydrogen nuclei (1H NMR $T_1(T)$), $D_3(S)$ and $D_3(R)$ forms of DABCO can make up a racemic mixture, and their mirror symmetry may be broken during the phase transition at ~ 60 K [6,11,12]. The time decay of nuclear magnetic moments (M) of hydrogen atoms in DABCO was analyzed to find the distribution of DABCO molecules over different states. Above ~ 165 K, the time decay of M is a single exponential function characterized by a single value T_1 . In this case, DABCO molecules with D_3 and D_{3h} symmetries reorient similarly, their proton spins constitute a single spin system, the activation barrier is equal to ~ 4 kJ/mol. Between 165 and 60 K, the time decay of M is a biexponential function containing two values T_1 , each corresponding to a certain fraction of nuclear spins in M . The ratio of these fractions is estimated to be $1/3:2/3$. The $1/3 \cdot M$ fraction corresponds to 1H spins of DABCO molecules of the D_{3h} symmetry, the mobility of which is characterized by a short value T_{1SH} . The $2/3 \cdot M$ fraction corresponds to 1H spins of the sum of S- and R-forms of DABCO. In this case, these forms are indistinguishable due to tunneling transitions, so the above fraction ($2/3 \cdot M$) represents the racemic state of DABCO molecules and is characterized by a single value T_{1L} of a larger magnitude. During

the phase transition at 60 K and down to 25 K, the behavior of T_{1L} is interpreted as the termination of tunneling between energy degenerate quantum states of R- and S- forms of DABCO, and their fractions in \mathbf{M} remain equal to each other ($1/3:1/3$). Below 25 K, the decay \mathbf{M} is nonexponential and can be conventionally characterized by three values T_1 . So, the phase transition at ~ 14 K is associated with the redistribution of DABCO molecules over different energy states characterized by contributions $1/4 \cdot \mathbf{M}$, $1/4 \cdot \mathbf{M}$, and $1/2 \cdot \mathbf{M}$ and the appearance of a chiral polarized state [11].

Note that the racemate state was also reported for 1,4-bis(carboxyethynyl)bicyclo[2.2.2]octane (BABCO) molecules, which are analogs of DABCO. It was shown that the ratio of left- and right-twisted forms of BABCO can be controlled by light [18,19]. The disorder of DABCO and its analogs, which causes phase transitions, is also observed in other systems [20–22].

Thus, the ^1H NMR $T_1(T)$ data testify that phase transitions are associated with the mobility of DABCO molecules. The analysis of the function \mathbf{M} provides quantitative data on the distribution of DABCO molecules over different states at various temperatures. However, it is still unclear how these states are structurally realized in Zn-DMOF. Low-temperature heat capacity data for Zn-DMOF may be used to clarify this problem.

4. Low-Temperature Heat Capacity in $\text{Zn}_2(\text{C}_8\text{H}_4\text{O}_4)_2 \cdot \text{C}_6\text{H}_{12}\text{N}_2$

All phase transitions in Zn-DMOF (at ~ 14 , ~ 60 , and ~ 130 K) are second-order phase transitions [10]. Table 1 shows the maximum values of the anomalous parts of heat capacity $\Delta C_p = C_p - C_p^L$, where C_p is the heat capacity of the substance and C_p^L is the regular part of heat capacity “in the absence of phase transitions”. The entropy of the phase transitions is shown in Table 2.

Table 1. ΔC_p (J/mol/K) values at the phase transitions in Zn-DMOF under various pressures of the heat-exchange gas ^4He ($P \cdot 10^5, \text{Pa}$).

P	~ 14 K	~ 60 K	~ 130 K
0.51	6.0 ± 0.4	8.0 ± 0.2	23.0 ± 0.3
1.52	5.0 ± 0.4	11.0 ± 0.2	23.0 ± 0.3

Table 2. Entropies $\Delta S/R$ of the phase transitions in the region of critical temperatures (T_c , K) under various pressures of the heat-exchange gas ^4He ($P \cdot 10^5, \text{Pa}$) in Zn-DMOF. R is the universal gas constant.

T_c	~ 14	~ 60	~ 130
P	$\Delta S/R$	$\Delta S/R$	$\Delta S/R$
0.51	0.42 ± 0.05	0.14 ± 0.02	0.30 ± 0.04
1.52	0.28 ± 0.04	0.23 ± 0.02	0.30 ± 0.04

The obtained data indicate that the absorbed atoms of ^4He affect the states of $\text{D}_3(\text{S})$ and $\text{D}_3(\text{R})$ forms of DABCO (phase transitions ~ 14 and ~ 60 K) and do not affect the ordering and disordering of BDC^{2-} anions during the phase transition at 130 K. This result can be explained by the fact that the structure of DABCO is flexible [23,24] as compared to that of BDC^{2-} anions and can therefore be deformed in the presence of adjoining ^4He atoms, whereas the structure of BDC^{2-} anions remains unchanged.

The temperature dependence of heat capacity of Zn-DMOF is almost linear between the phase transitions at ~ 14 , ~ 60 , and ~ 130 K and above 130 K [8,10,11] to indicate the presence of a one-dimensional elastic continuum [8,12]. Figure 2 shows the comparison of experimental [8] and tabulated (Tarasov model) [25,26] heat capacity values using the fitting parameters obtained in [11].

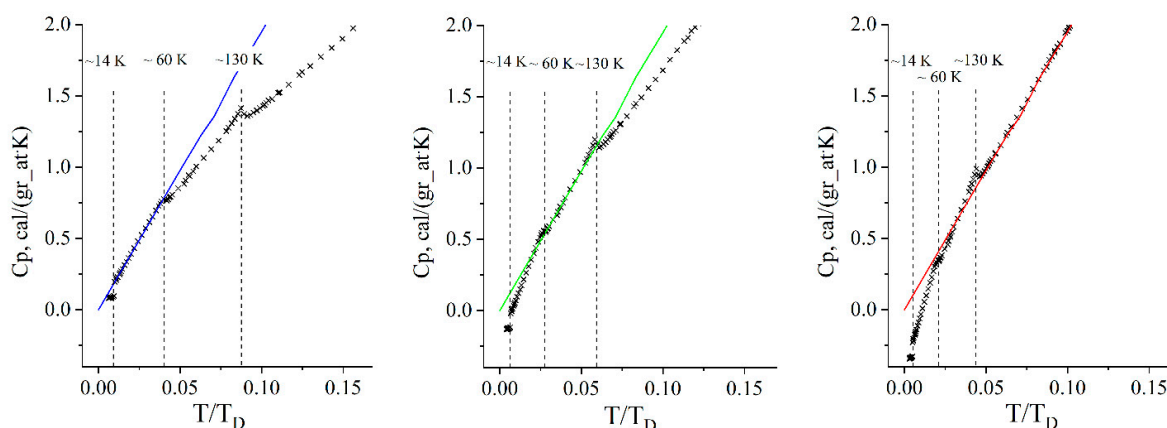


Figure 2. Tabulated (T/T_D) experimental (+) and calculated (solid lines) dependences of heat capacity (C_p) for Zn-DMOF and one-dimensional elastic continuums (Tarasov model [25]). Vertical dashed lines show the temperatures of phase transitions. Solid blue, green, and red lines corresponds to the Debye temperatures of 1490 K, 2230 K, and 2950 K, respectively (according to the data reported in [11]).

According to the XRD data, the crystal lattice of Zn-DMOF expands along the **a** and **b** axes ($dL/LdT(\mathbf{a,b}) = -9.59 \cdot 10^{-6} \text{ K}^{-1}$) and shrinks along the **c** axis ($dL/LdT(\mathbf{c}) = 12.2 \cdot 10^{-6} \text{ K}^{-1}$) as the temperature decreases to $\sim 130 \text{ K}$ and below $\sim 130 \text{ K}$ ($|dL/LdT(\mathbf{c})| > |dL/LdT(\mathbf{a,b})|$ (dL/LdT is the coefficient of thermal expansion) [9]. Hence, the interactions in the $-\text{Zn-DABCO-Zn}-$ chain directed along the **c** axis are assumingly stronger than $\text{BDC}^{2-}-[\text{Zn}_2]^{4+}-\text{BDC}^{2-}$ interactions in the **ab** plane, which determines a one-dimensional elastic continuum for the behavior of the heat capacity. The phase transition at $\sim 130 \text{ K}$ was interpreted as an order-disorder phase transition associated with a change in the relative spatial arrangement of BDC^{2-} anions, while the DABCO molecules preserve their activation mobility and remain disordered [9].

Linear regions of heat capacity in Zn-DMOF were analyzed using the Stockmayer-Hecht model for the heat capacity of chain crystalline polymers [26,27]. The model assumes that molecular groups in a chain vibrate as single units connected by strong intrachain bonds, while interchain interactions are neglected. The temperature dependence of the volumetric heat capacity C_v is expressed in terms of two relationships, $C_v/(3Nk)$ and T/T_m , where N is the number of repeated vibrating units, $T_m = h\nu_m/k$, h is the Planck constant, k is the Boltzmann constant, and ν_m is the maximum frequency of stretching vibrations in the chain. The repeated vibrating unit along the **c** axis in Zn-DMOF consists of two Zn atoms and one DABCO molecule ($\{\text{Zn}_2\text{DABCO}\}$) [5].

Experimental smoothed values C_p obtained as functions of temperature in [8] were represented on a log-log plot and fitted by best tabulated values $C_v/(3Nk)$ for each T/T_m assuming that $C_p - C_v$ is small [27] (Figure 3). As a result, it was found that the vibrating chain is formed by $\sim 38\text{--}39$ $\{\text{Zn}_2\text{DABCO}\}$ units above 130 K, by ~ 30 units at 60–130 K, and by ~ 12 units at 14–60 K (Table 3). Below 14 K, the heat capacity obeys the $\sim T^3$ law (Figure 3) to indicate that interchain interactions become stronger and the lattice vibrational modes become three-dimensional [8,25].

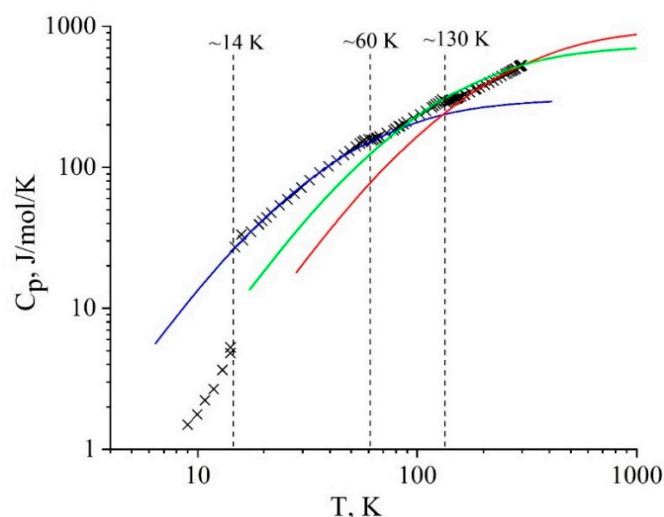


Figure 3. Log-log plot of the Zn-DMOF heat capacity versus temperature. Experimental (crosses) and calculated values of heat capacity at 14.7–57.4 K (blue lines), 130.1–72.6 K (green lines), and 299.6–141.6 K (red lines).

Table 3. Calculated parameters for Zn-DMOF. **M** is the nuclear magnetic moment, **N** is the number of {Zn₂DABCO} units normalized with respect to corresponding values above 130 K.

Region of Fit, K	299.6–141.6	130.1–72.6	57.4–14.7
ν_m, cm^{-1}	1250	765	285
N	~38.5	~28.9	~12.0
N	1	~0.75	~0.31
M	1	~0.67	~0.33

The values $\nu_m \sim 1250 \text{ cm}^{-1}$ and $\nu_m \sim 765 \text{ cm}^{-1}$ fall into the region of stretching vibrations of DABCO, and $\nu_m \sim 285 \text{ cm}^{-1}$ fall into the region of Zn-N and Zn-Zn stretchings (Table 3) [28]. Thus, the obtained values ν_m correspond to the stretchings in the chains, in accordance with the model [27].

As can be seen, the values obtained from the analysis of C_p for **N** {Zn₂DABCO} units correlate with fractions (**M**) in different phases of Zn-DMOF, if **N** and **M** values above 130 K are taken as a unit (Table 3). The obtained quantitative agreement between NMR data and the analysis of heat capacity suggests the following conclusions. Above 130 K, the chains consisting of ~39 {Zn₂DABCO} units contain DABCO molecules with D₃(S), D₃(R), and D_{3h} symmetries. At 60–130 K, the longest chains (~29 {Zn₂DABCO} units) contain only D₃ forms in the racemic state. The vibrations of these chains make the largest contribution to the heat capacity, while the vibrations of the chains consisting of D_{3h} forms make no contribution practically, due to their shorter size. Finally, below ~60 K there are three types of chains (~12 {Zn₂DABCO} units) of the same length but containing three different DABCO forms (D₃(S), D₃(R), and D_{3h}). The size of the chains below 14 K cannot be estimated, since the heat capacity is no more linear at these temperatures.

5. Heat Capacity Behavior during the Phase Transition at 60 K and the Salam Hypothesis

The PVED values for the DABCO molecule and the [Zn₂DABCO]⁴⁺ cation were obtained in [29]. The difference between the energies of mirror isomers is as small as $\sim 5 \cdot 10^{-16} \text{ kJ/mol}$ ($\sim 5.2 \cdot 10^{-18} \text{ eV}$) for DABCO and an order of magnitude higher ($\sim 5 \cdot 10^{-15} \text{ kJ/mol}$ or $\sim 5.2 \cdot 10^{-17} \text{ eV}$) for the [Zn₂DABCO]⁴⁺ cation. Therefore, the contribution of PVED increases in the presence of Zn²⁺ cations and is determined mainly by the contribution of zinc cations. This contribution increases if Zn²⁺ cations are replaced by heavier cations Cd²⁺ and Hg²⁺ [30]. Hence, it can be assumed that the PVED breaking of mirror

symmetry between $D_3(S)$ and $D_3(R)$ forms of DABCO may be caused by their external environment in the Zn-DMOF structure.

If the symmetry breaking during the phase transition at ~ 60 K takes place in the chains containing only $D_3(S)$ and $D_3(R)$ forms of DABCO, then, according to the Salam hypothesis, the behavior of heat capacity must correspond to the behavior of heat capacity during the superconducting phase transition [1,2].

In fact, it was discovered that the temperature behavior of heat capacity of Zn-DMOF is an exponential function below ~ 60 K (Figure 4) [31]. The behavior of heat capacity in the region of second-order phase transitions was studied using the values of the anomalous part of heat capacity $\Delta C_p = C_p - C_p^L$, and the behavior of C_p^L was described using the Tarasov model [25]. Figure 3 shows the obtained ΔC_p values.

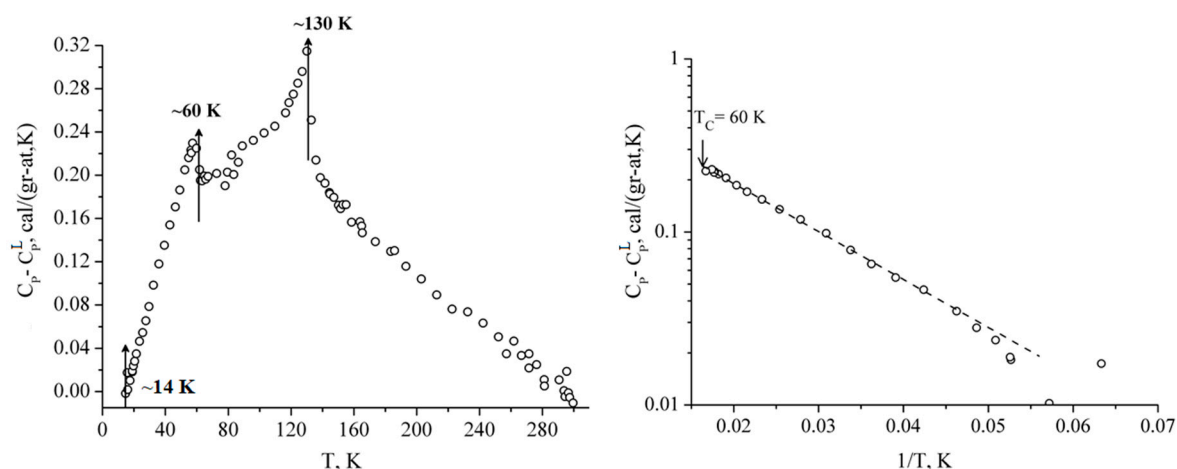


Figure 4. Temperature dependence of ΔC_p (in gram-atom units) for Zn-DMOF (left) and ΔC_p plotted as a function of $1/T$ below ~ 60 K (right). ΔC_p is shown on the logarithmic scale (according to the data from Figures 2 and 4 in [31]).

The region below ~ 60 K is of particular interest, since it is associated with the termination of tunneling between $D_3(S)$ and $D_3(R)$ forms of DABCO as the temperature decreases [11,12]. Based on the hypothesis suggested in [1,2], a study was carried out to verify the compliance of heat capacity ΔC_p to the exponential dependence $\sim \exp(-\Delta/T)$, где $\Delta = 1.76 \cdot T_c$ (Δ is the energy gap at 0 K). Figure 4 shows ΔC_p as a function of $1/T$ in the temperature region $15 \text{ K} < T < 60 \text{ K}$. As can be seen, a good agreement with the exponential law is achieved for the parameter Δ equal to $\sim 56 \text{ K}$ (or $\sim 5 \cdot 10^{-3} \text{ eV}$) [31]. The obtained value Δ turned out to be almost twice as small as expected ($\sim 106 \text{ K}$ for $T_c = 60 \text{ K}$). There is probably some inaccuracy with the parameters determining function C_p^L , which may cause the error of determining the Δ value. However, the detected exponential behavior of ΔC_p below 60 K signifies the presence of a BE condensation. The amplitude of ΔC_p during the phase transition at is $60 \text{ K} \approx 10 \text{ J/mol/K}$ (Table 1), which corresponds to the thermal energy jump $(\Delta C_p \cdot T_c) \approx 600 \text{ J/mol}$ (or $6 \cdot 10^{-3} \text{ eV}$), which agrees well with Δ . The value of $(\Delta C_p \cdot T_c)$ is 10^{15} times bigger than the PVED ($\sim 5.2 \cdot 10^{-18} \text{ eV}$) of one DABCO molecule, but it can be explained by the phenomenon of BE condensation [1,2].

However, neither C_p data nor ^1H NMR $T_1(T)$ data show any energy difference between $D_3(S)$ and $D_3(R)$ forms of DABCO below 60 K (according to the Salam hypothesis, the ratio between $D_3(S)$ and $D_3(R)$ forms of DABCO should change). Apparently, the energy difference between $D_3(S)$ and $D_3(R)$ forms remains negligible and can be observed only at lower temperatures, when the thermal energy of the crystal approaches zero [6]. Indeed, according to ^1H NMR $T_1(T)$ data, the decay M as a function of time shows anomalous behavior below 25 K [12], but it is not manifested in the C_p behavior until the phase transition at $\sim 14 \text{ K}$.

6. Conclusions

The Salam hypothesis is considered impossible during the phase transitions in amino acid crystals, since the barriers between L- and D-forms of alanine involve intramolecular bond breaking and are as high as ~200 kJ/mol [32]. In Zn-DMOF, the activation barrier between D₃(S) and D₃(R) forms of DABCO is estimated to be ~4 kJ/mol [7] and 5 kJ/mol [27] according to NMR data and quantum chemical calculations, respectively. Thus, this barrier is ~40 times smaller than the barrier between L- and D-forms of alanine [30]. The NMR data indicate the presence of tunneling between D₃(S) and D₃(R) forms of DABCO. The tunneling splitting for the DABCO molecule in the free state is estimated to be ~6 cm⁻¹ (~8.6 K) [24], which is comparable to the temperature range of observed phase transitions in Zn-DMOF. The behavior of heat capacity below 60 K corresponds to the heat capacity during the BE condensation. According to the NMR data, still lower temperatures are associated with a redistribution of DABCO with different symmetries over energy states to form a chiral polarized state. In the model system [Zn₂DABCO]⁴⁺, the R-form is most favorable due to the PVED [29,30], but it is currently unclear which symmetry of the chains built of {Zn₂DABCO} units corresponds to the most energetically favorable state. The method of resonant X-ray diffraction with circularly polarized X-rays [33] or optical methods seem to be most preferable for use at low and extra-low temperatures.

We believe that metal-organic frameworks or related compounds containing enantiomers in the racemic state (not necessarily amino acid molecules) may be considered as model systems to study Salam phase transitions. Our studies were aimed at revealing the effects of chirality stabilization in isomeric molecules in solids at low temperatures with the goal of exploring the idea of the cold scenario of life origin on the Earth.

Author Contributions: S.K., analysis of heat capacity data, writing and editing of the manuscript, M.R., editing of the manuscript and discussion, D.P., discussion, I.M.: discussion.

Funding: This research received no external funding.

Conflicts of Interest: The authors declare no conflict of interest.

References

1. Salam, A. The role of chirality in the origin of life. *J. Mol. Evol.* **1992**, *33*, 105–113. [[CrossRef](#)]
2. Salam, A. Chirality, phase transitions and their induction in amino acids. *Phys. Lett. B* **1992**, *288*, 153–160. [[CrossRef](#)]
3. Bargueño, P.; Perez de Tudela, R.; Miret-Artés, S.; Gonzalo, I. An alternative route to detect parity violating energy differences through Bose–Einstein condensation of chiral molecules. *Phys. Chem. Chem. Phys.* **2011**, *13*, 806–810. [[CrossRef](#)] [[PubMed](#)]
4. Kozlova, S.G.; Mirzaeva, I.V.; Ryzhikov, M.R. DABCO molecule in the M₂(C₈H₄O₄)₂·C₆H₁₂N₂ (M = Co, Ni, Cu, Zn) metal-organic frameworks. *Coord. Chem. Rev.* **2018**, *376*, 62–74. [[CrossRef](#)]
5. Dybtsev, D.N.; Chun, H.; Kim, K. Rigid and flexible: A highly porous metal–organic framework with unusual guest-dependent dynamic behavior. *Angew. Chem. Int. Ed.* **2004**, *43*, 5033–5036. [[CrossRef](#)]
6. Kozlova, S.G.; Gabuda, S.P. Thermal properties of Zn₂(C₈H₄O₄)₂·C₆H₁₂N₂ metal-organic framework compound and mirror symmetry violation of dabco molecules. *Sci. Rep.* **2017**, *7*, 11505. [[CrossRef](#)]
7. Gabuda, S.P.; Kozlova, S.G.; Samsonenko, D.G.; Dybtsev, D.N.; Fedin, V.P. Quantum Rotations and Chiral Polarization of Qubit Prototype Molecules in a Highly Porous Metal–Organic Framework: ¹H NMR T₁ Study. *J. Phys. Chem. C* **2011**, *115*, 20460–20465. [[CrossRef](#)]
8. Paukov, I.E.; Samsonenko, D.G.; Pishchur, D.P.; Kozlova, S.G.; Gabuda, S.P. Phase transitions and unusual behavior of heat capacity in metal organic framework compound Zn₂(C₈H₄O₄)₂ N₂(CH₂)₆. *J. Solid State Chem.* **2014**, *220*, 254–258. [[CrossRef](#)]
9. Kim, Y.; Haldar, R.; Kim, H.; Koo, J.; Kim, K. The guest-dependent thermal response of the flexible MOF Zn₂(BDC)₂(DABCO). *Dalton Trans.* **2016**, *45*, 4187–4192. [[CrossRef](#)] [[PubMed](#)]
10. Pishchur, D.P.; Kompankov, N.B.; Lysova, A.A.; Kozlova, S.G. Order-disorder phase transitions in Zn₂(C₈H₄O₄)₂·C₆H₁₂N₂ in atmospheres of noble gases. *J. Chem. Thermodyn.* **2019**, *130*, 147–153. [[CrossRef](#)]

11. Gabuda, S.P.; Kozlova, S.G. Chirality-related interactions and a mirror symmetry violation in handed nano structures. *J. Chem. Phys.* **2014**, *141*, 044701. [[CrossRef](#)]
12. Gabuda, S.P.; Kozlova, S.G. Abnormal difference between the mobilities of left- and right-twisted conformations of $C_6H_{12}N_2$ roto-symmetrical molecules at very low temperatures. *J. Chem. Phys.* **2015**, *142*, 234302. [[CrossRef](#)]
13. Sabylnskii, A.V.; Gabuda, S.P.; Kozlova, S.G.; Dybtsev, D.N.; Fedin, V.P. 1H NMR refinement of the structure of the guest sublattice and molecular dynamics in the ultrathin channels of $[Zn_2(C_8H_4O_4)_2(C_6H_{12}N_2)] \cdot n(H_3C)_2NCHO$. *J. Struct. Chem.* **2009**, *50*, 421–428. [[CrossRef](#)]
14. Gallyamov, M.R.; Moroz, N.K.; Kozlova, S.G. NMR line shape for a rectangular configuration of nuclei. *Appl. Magn. Reson.* **2011**, *41*, 477–482. [[CrossRef](#)]
15. Khudozhnikov, A.E.; Kolokolov, D.I.; Stepanov, A.G.; Bolotov, V.A.; Dybtsev, D.N. Metal-cation-independent dynamics of phenylene ring in microporous MOFs: A 2H solid-state NMR study. *J. Phys. Chem. C* **2015**, *119*, 28038–28045. [[CrossRef](#)]
16. Kozlova, S.G.; Pishchur, D.P.; Dybtsev, D.N. Phase transitions in a metal–organic coordination polymer: $[Zn_2(C_8H_4O_4)_2(C_6H_{12}N_2)]$ -with guest molecules. Thermal effects and molecular mobility. *Phase Trans.* **2017**, *90*, 628–636. [[CrossRef](#)]
17. Burtch, N.C.; Torres-Knoop, A.; Foo, G.S.; Leisen, J.; Sievers, C.; Ensing, B.; Dubbeldam, D.; Walton, K.S. Understanding DABCO nanorotor dynamics in isostructural metal–organic frameworks. *J. Phys. Chem. Lett.* **2015**, *6*, 812–816. [[CrossRef](#)] [[PubMed](#)]
18. Lemouchi, C.; Mézière, C.; Zorina, L.; Simonov, S.; Rodríguez-Forteza, A.; Canadell, E.; Wzietek, P.; Auban-Senzier, P.; Pasquier, C.; Giamarchi, T.; et al. Design and evaluation of a crystalline hybrid of molecular conductors and molecular rotors. *J. Am. Chem. Soc.* **2012**, *134*, 7880–7891. [[CrossRef](#)]
19. Lemouchi, C.; Iliopoulos, K.; Zorina, L.; Simonov, S.; Wzietek, P.; Cauchy, T.; Rodríguez-Forteza, A.; Canadell, E.; Kaleta, J.; Michl, J.; et al. Crystalline arrays of pairs of molecular rotors: Correlated motion, rotational barriers, and space-inversion symmetry breaking due to conformational mutations. *J. Am. Chem. Soc.* **2013**, *135*, 9366–9376. [[CrossRef](#)]
20. Shi, X.; Luo, J.; Sun, Z.; Li, S.; Ji, C.; Li, L.; Han, L.; Zhang, S.; Yuan, D.; Hong, M. Switchable dielectric phase transition induced by ordering of twisting motion in 1,4-diazabicyclo[2.2.2]octane chlorodifluoroacetate. *Cryst. Growth Des.* **2013**, *13*, 2081–2086. [[CrossRef](#)]
21. Yao, Z.-S.; Yamamoto, K.; Cai, H.-L.; Takahashi, K.; Sato, O. Above room temperature organic ferroelectrics: Diprotonated 1,4-diazabicyclo[2.2.2] octane shifts between two 2-chlorobenzoates. *J. Am. Chem. Soc.* **2016**, *138*, 12005–12008. [[CrossRef](#)]
22. Chen, L.-Z.; Huang, D.-D.; Ge, J.-Z.; Pan, Q.-J. Reversible ferroelastic phase transition of N-chloromethyl-1,4-diazabicyclo[2.2.2]octonium trichlorobromoquo copper(II). *Inorg. Chem. Commun.* **2014**, *45*, 5–9. [[CrossRef](#)]
23. Nizovtsev, A.S.; Ryzhikov, M.R.; Kozlova, S.G. Structural flexibility of DABCO. Ab initio and DFT benchmark study. *Chem. Phys. Lett.* **2017**, *667*, 87–90. [[CrossRef](#)]
24. Mathivon, K.; Linguerri, R.; Hochlaf, M. Systematic theoretical studies of the interaction of 1,4-diazabicyclo [2.2.2]octane (DABCO) with rare gases. *J. Chem. Phys.* **2013**, *139*, 164306.
25. Tarasov, V.V. Heat Capacity of Anisotropic Solids. *Zhurnal Fiz. Khimii* **1950**, *24*, 111–128. (In Russian)
26. Wunderlich, B.; Baur, H. *Heat Capacities of Linear High Polymers*; Springer: Berlin, Germany, 1970.
27. Stockmayer, W.H.; Hecht, C.E. Heat capacity of chain polymeric crystals. *J. Chem. Phys.* **1953**, *21*, 1954–1958. [[CrossRef](#)]
28. Tan, K.; Nijem, N.; Canepa, P.; Gong, Q.; Li, J.; Thonhauser, T.; Chabal, Y.J. Stability and hydrolyzation of metal organic frameworks with paddle-wheel SBUs upon hydration. *Chem. Mater.* **2012**, *24*, 3153–3167. [[CrossRef](#)]
29. Mirzaeva, I.V.; Kozlova, S.G. Computational estimation of parity violation effects in a metal-organic framework containing DABCO. *Chem. Phys. Lett.* **2017**, *687*, 110–115. [[CrossRef](#)]
30. Mirzaeva, I.V.; Kozlova, S.G. Parity violating energy difference for mirror conformers of DABCO linker between two M^{2+} cations ($M = Zn, Cd, Hg$). *J. Chem. Phys.* **2018**, *149*, 214302. [[CrossRef](#)] [[PubMed](#)]
31. Kozlova, S.G. Behavior of the heat capacity at second-order phase transitions in the $[Zn_2(C_8H_4O_4)_2 \cdot C_6H_{12}N_2]$ metal-organic framework compound. *JETP Lett.* **2016**, *104*, 253–256. [[CrossRef](#)]

32. Sullivan, R.; Pyda, M.; Pak, J.; Wunderlich, B.; Thompson, J.R.; Pagni, R.; Pan, H.J.; Barnes, C.; Schwerdtfeger, P.; Compton, R. Search for electroweak interactions in amino acid crystals. II. The Salam hypothesis. *J. Phys. Chem. A* **2003**, *107*, 6674–6680. [[CrossRef](#)]
33. Tanaka, Y.; Kojima, T.; Takata, Y.; Chainani, A.; Lovesey, S.W.; Knight, K.S.; Takeuchi, T.; Oura, M.; Senba, Y.; Ohashi, H.; et al. Determination of structural chirality of berlinite and quartz using resonant x-ray diffraction with circularly polarized x-rays. *Phys. Rev. B* **2010**, *81*, 144104. [[CrossRef](#)]



© 2019 by the authors. Licensee MDPI, Basel, Switzerland. This article is an open access article distributed under the terms and conditions of the Creative Commons Attribution (CC BY) license (<http://creativecommons.org/licenses/by/4.0/>).